UCRL-JC-139459
PREPRINT

# NIF-scale hohlraum asymmetry studies using point-projection radiograph of thin shells

Steve Pollaine, David Bradley, Otto Landen, Russell Wallace,
Ogden Jones, Peter Amendt, Larry Suter and Robert Turner

Lawrence Livermore National Laboratory
Livermore, CA 94550

This paper was prepared for submittal to
42nd Annual Meeting of the APS Division of Plamsa Physics
Quebec City, Canada
October 23-27, 2000

**October 18, 2000**

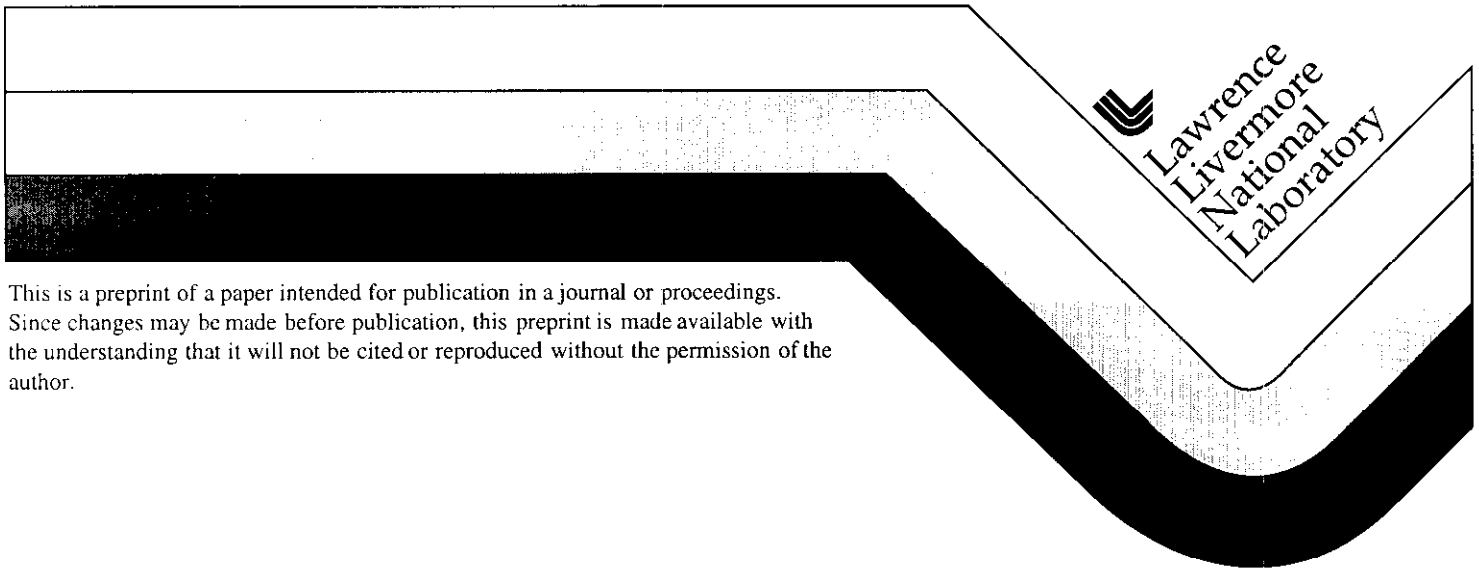

# National Ignition Facility-scale hohlraum asymmetry studies by thin shell radiography

Steve Pollaine, David Bradley, Otto Landen, Russell Wallace,

Ogden Jones, Peter Amendt, Larry Suter and Robert Turner

Lawrence Livermore National Laboratory

## Abstract

A necessary condition for igniting indirectly-driven inertial confinement fusion (ICF) capsules on the National Ignition Facility (NIF) is controlling drive asymmetry to the 1% level [S. W. Haan, S. M. Pollaine, J. D. Lindl *et al*., "Design and modeling of ignition targets for the National Ignition Facility," Physics of Plasmas **2**, 2480-7 (1995)]. Even flux-asymmetry modes (e.g. Legendre modes $P_2$,$P_4$, $P_6$ and $P_8$) must be reduced by hohlraum design and laser beam pointing. Odd flux-asymmetry modes (e.g. Legendre modes $P_1$, $P_3$, $P_5$, etc.) are theoretically removed by reflection symmetry across the hohlraum midplane [S. M. Pollaine and D. Eimerl, "Modal analysis of power imbalance and pointing errors for direct drive and tetrahedral hohlraums," Nuclear Fusion **38** (10), 1523-30 (1998)], but will be produced by power imbalance, laser beam pointing errors, and target fabrication errors. We are now conducting an experimental campaign on the University of Rochester's Omega laser to measure higher order ($P_4$ and higher) flux asymmetry modes inside hohlraums that approximate the conditions of a NIF hohlraum during the 90-eV early drive phase[S. W. Haan, S. M. Pollaine, J. D. Lindl *et al*., "Design and modeling of ignition targets for the National Ignition Facility," Physics of Plasmas **2**,

2480-7 (1995)]. These experiments use a new point-projection backlighting technique to cast high quality 4.7 keV radiographs of thin 2 mm diameter Ge-doped CH shells designed to enhance sensitivity to drive asymmetries. Distortions in the position of the limb of the shells resulting primarily from drive asymmetries are measured to an accuracy of 2 μm. The linearity and sensitivity of thin imploding shells to flux asymmetry makes it possible to achieve this degree of accuracy, which is sufficient for NIF ignition symmetry tuning. The promising results to date allow us to compare measured and predicted distortions and by inference drive asymmetries for the first 8 asymmetry modes.

## I. Introduction

The National Ignition Facility (NIF) is a 192 beam, 2 MJ 0.35 μm laser now being built at Lawrence Livermore National Laboratory [1]. NIF is designed to drive inertial confinement fusion (ICF) capsules to ignition using indirect drive, in which the laser energy is converted to thermal x rays inside a cavity (hohlraum). The x rays then ablate the outer layers of a capsule inside the hohlraum, causing the capsule to implode and

achieve ignition. One of the major sources of possible failure to achieve ignition is x-ray flux asymmetry on the capsule. All flux asymmetry can be analyzed in terms of the spherical harmonics $Y_{lm}$. If the flux is azimuthally symmetric (such as in the NIF baseline cylindrical hohlraum illuminated by rings of beams), only the m=0 components exist and the flux asymmetry can be expressed in terms of the Legendre polynomials $P_l$. In this paper, we will describe flux asymmetry in terms of the Legendre polynomial coefficients $a_l$.

Because the cylindrical hohlraum is symmetric about the midplane, odd Legendre modes are zero in the absence of pointing errors and power imbalance. Because higher modes are smoothed out by radiation transport from the hohlraum walls to the capsule (with a transfer function that goes roughly as $mode^{-2.5}$ [2]), we are most concerned with diagnosing and controlling $P_2$, $P_4$, $P_6$ and $P_8$ flux asymmetry (See Sec. VIII. for details).

Fig. 1 shows a typical NIF ignition capsule and the temperature drive profile. Typically, three or four shocks keep the DT fuel on a low adiabat, so that the capsule may reach roughly 1000 g/cc at ignition time. In addition, the fuel must be compressed symmetrically to ensure such a high fuel density. For example, 2-D integrated radiation-hydrodynamics simulations [3] show that the capsule will fail when the average Legendre coefficient $a_6$ is greater than 1% of $a_0$, or when $a_8$ is greater than 0.6% of $a_0$, as illustrated in Fig. 2. To provide for some margin of error, we have set the NIF specifications on flux asymmetry as $a_2/a_0 < 1.0\%$, $a_4/a_0 < 0.5\%$, $a_6/a_0 < 0.3\ \%$, and $a_8/a_0 < 0.25\%$ [4]. Fig. 3 shows the Legendre coefficients as a function of time for one of our NIF integrated

radiation hydrodynamic simulations. This simulation has not been fully optimized for flux symmetry.

## II. Asymmetry Diagnostics

A variety of different techniques measure the symmetry in hohlraums using surrogate capsules. The reemission ball [5] is a solid high Z (e.g. Bi) ball placed in the same central location as an ICF capsule. Thermal radiation on the ball heats up its surface, and it reemits as a blackbody at some slightly lower temperature, which will vary from point to point on the ball if the incoming flux is asymmetric. When viewed in for example 2 keV x rays, the re-emission from the ball is highly sensitive to fluctuations around the characteristic 90-300 eV incoming NIF drive temperatures. Thus small variations in incoming flux are magnified, and can be measured as a function of time.

Another asymmetry diagnostic is the foam ball [6]. This is a solid sphere of low-density $SiO_2$ or CH. A converging shock produces a visible limb, and the radius of the limb as a function of angle gives information about the incoming flux asymmetry as a function of time. The speed of the shock varies as the square root of the incident flux and as the inverse square root of the foam ball density, explaining why the sensitivity of the technique is optimized by using foam (i.e. low densities).

A third asymmetry diagnostic is the imaging of imploded cores from a surrogate capsule. For example, spherical hohlraums with tetrahedral illumination (four laser entrance holes) have yielded triangular implosion images [7], showing that the part of the capsule that lies under a laser entrance hole feels a reduced flux. The thickness of the

capsule shell can be varied to vary the sampling time [8]. In this paper, we will concentrate on the latest addition to the array of symmetry diagnosis techniques, the thin shell diagnostic. Table 1 below compares the demonstrated accuracy of the various techniques for $P_2$, $P_4$, $P_6$ and $P_8$.

## III. Thin shell asymmetry diagnostic

The thin shell diagnostic is a capsule with a radius $r_0$ equal to or slightly larger relative to the hohlraum radius than for the NIF capsule, and having a thickness of 10 to 100 μm of doped plastic. A slightly larger radius enhances the imprinting of higher order modes (e.g $P_6$ and $P_8$) as discussed later. The dopant (in this case Ge) provides radiographic contrast and mitigates the effects of decompression due to preheat. Because the acceleration is proportional to the ablation pressure divided by the areal mass density $\int \rho dr$, and $\int \rho dr$ is approximately conserved during the implosion, the shape of the thin-shell capsule reflects the drive asymmetry. Thus there is less non-linear coupling between the different modes, compared to shock-driven surrogates such as solid foam balls. This is important because large but tolerable swings in $P_2$ (e.g. 10% over 2 ns) won't couple to the higher order modes we want to measure with the thin shell.

A useful measure of linearity is the coefficient c in $\frac{d\alpha}{\alpha} = c\frac{\mathrm{dF}}{\mathrm{F}}$, where α is the measured observable (re-emitted flux F for re-emission sphere and distance traveled d for the foam ball and thin shell diagnostics) and $T^4$ is the flux driving the implosion (or pressure for thin shell and foam ball). In a strictly linear system, c = 1. For a foam ball, c

= 1/2 because $r \sim \int\sqrt{(P_r)}dt$ since the shocked particle speed $\sim \sqrt{P_r}$. For the reemission balls, we replace radius and pressure with the re-emitted flux F(hν) and incoming flux $T^4$. For a pure blackbody, F~exp(-hν/kT), so that $\frac{dF}{F} = \frac{1}{4}\frac{h\nu}{kT}\frac{dT^4}{T^4}$. For example, for a 200 eV hohlraum and hν = 2 keV, then c = 2.5. For a thin shell, c = 1 as long as $\int \rho dr$ is constant. This approximation is good, as the increase in $\int \rho dr$ due to convergence tends to cancel the decrease in $\int \rho dr$ due to mass ablation, at least until the shell has converged by a factor of 2.

Note that the measurement of flux asymmetry depends on the areal mass density being constant over angle, not over time. As mass is ablated, the areal mass density decreases. This decrease is enhanced where the flux is stronger. Then the acceleration will increase both because of the stronger flux and the decreased areal mass density. Because of this non-linear amplification, c increases from 1 to roughly 1.2.

Another way that nonlinearity could develop is if mass flowed in a transverse direction due to the Rayleigh-Taylor instability [9]. Most of these models of Rayleigh-Taylor growth assume an incompressible fluid (with or without density gradients), which implies an infinite sound speed. In our experiments described below, the sound speed in the driven shell is less than 30 μm/ns. In the relevant 4.5 ns time interval, pressure inhomogeneities will propagate no more than 135 μm. For the shortest asymmetry mode of interest, mode 8, the initial wavelength for the 800 μm shells used was 630 μm. Becaues pressure inhomogeneities can travel only one fifth of a wavelength in the transverse dimension, there is not enough time for the Rayleigh-Taylor instability to grow. This lack of Rayleigh-Taylor growth is confirmed by 2-D hydrodynamic

simulations [3]. These show no growth beyond what is expected from a rocket model [10], which has the nonlinear amplification discussed in the preceding paragraph.

In a thin shell, the outer part of the shell ablates, compressing the inner part of the shell. For a typical CH(Ge) shell of $\rho \approx 1.3$ g/cc driven by the 90 eV foot drive of the NIF ignition hohlraum , the shell experiences a 1.2 to 1.4 Mb shock with a velocity jump of 8 to 9 μm/ns. When the shock reaches the inside edge of the shell (at about $t_0 = 1.4$ ns for a 15 μm thick shell), the shell starts accelerating. The motion of the dense shell is then given by

$$\mathrm{d} = r_0 - r(t) = v_0(t - t_0) + \int_{t_0}^{t} g(t')(t - t')dt', \quad g \propto \frac{\mathrm{Tr}^{3.5}}{\int \rho dr} \tag{1}$$

where $r_0 \sim 800$ μm, $v_0 \sim 9$ μm/ns, $t_0 \sim 1.4$ ns, and g is the acceleration resulting from typical low Z fully ionized material ablation.

These parameters allow us to calculate the sensitivity of the shell as a function of the time of the flux asymmetry. If the flux asymmetry occurs before shock break out time, then $v_0$ and $t_0$ are affected, and at late time the shell asymmetry will reflect the $v_0(t\text{-}t_0)$ term. If the flux asymmetry occurs after shock break out time, then the acceleration g is affected, and at late time the shell asymmetry will reflect the integral of the g term, which is much greater. Fig. 4 illustrates this point by showing the response of the shell asymmetry at 8 ns as a function of when the flux asymmetry is applied. Note that the radial position of the shell is most sensitive to asymmetry that occurs just after shock break out time $t_0$.

As the shell implodes, distortions caused by early flux asymmetry will continue to grow, even if the flux asymmetry disappears [see Eq. (1)]. Conversely, the last term in

Eq. (1) also shows that there can be some time integration of persisting asymmetries. This means that the thin shell technique is less well suited to measuring modes whose amplitude and/or sign change rapidly in time (e.g. with period $\tau$ shorter than the duration of the acceleration before a measurement is taken). This is particularly true of the $P_2$ component (for which a not applicable (NA) has been inserted in Table 1 under thin shell). The more instantaneous records of asymmetry provided by the foam ball or re-emission technique are more applicable for measuring the $P_2$ swings. Fortunately, the higher order modes such as $P_6$ and $P_8$ tend to remain at near constant values for many ns in NIF ignition hohlraum simulations (see Fig. 3), making them ideally suited for measurement by the thin shell technique.

The thickness of the shell can be varied to change the sampling time. However, if the shell is too thin, the Rayleigh-Taylor instability (with modes > 400) will break up the shell, and resolution of the limb will suffer. Our experiments suggest that an initial thickness of 15 μm is optimum for the shell travel distance of 200 μm observed in the experiments we are doing on the Omega laser at the Laboratory for Laser Energetics at the University of Rochester.

We can increase the capsule/case ratio to enhance the effect of high-order flux asymmetries. Fig. 5 shows the radiation transfer function for a capsule within a spherical case for a capsule/case radii ratio of 0, 0.2, 0.4, and 0.6 in modes 0 through 8. Note that by increasing the capsule/case ratio from a NIF-like value of 0.4 to 0.6, the sensitivity to modes 6 and 8 are increased by an order of magnitude. The transfer function for a sphere inside a cylinder, the usual hohlraum shape, is more complicated because the Legendre polynomials and spherical harmonics are no longer the normal modes. However, when

cross-coupling between modes is taken into account, there is still an order of magnitude increase in flux sensitivity to the higher modes with the higher capsule/case ratio. It should also be noted that Fig. 5 implies a strong reduction in transfer function as the shell implodes, which means that the sampling time for high order modes is even more peaked at just after shock break-out time, as illustrated in Fig 4.

2-D radiation-hydrodynamics simulations [3] show that a driven thin shell magnifies thickness variations, but not ripples on the surface that keep the thickness constant. For example, a 0.1 μm variation in thickness in a 15 μm shell that travels 200 μm will cause a distortion of 1.3 μm in radius, just below the limit of detectability.

## IV. Experiments on Omega

We have run four sets of experiments with the thin shell diagnostic at the 60-beam Omega laser at the Laboratory for Laser Energetics at the University of Rochester. These experiments are designed to emulate the foot drive of the NIF ignition hohlraum (see Fig. 1) while operating at close to NIF spatial scale to enhance detectability of shell distortions. The capsule-to-case radii ratios are chosen to be between 0.5 and 0.6 to enhance sensitivity to higher order modes ($P_6$ and $P_8$). In addition, the latest designs have incorporated a predicted non-negligible few % $P_6$ flux asymmetry component by appropriate choice of beam pointing. Fig. 6 shows the basic arrangement. The hohlraum is driven by several rings of laser beams at 23°, 48°, 59° and 62° relative to the hohlraum symmetry axis. Twenty-four of the 60 beams heat the hohlraum from 0 to 3 ns, and another 18 beams continue the heating from 3 to 6 ns. The staggering of beams is imposed by the 3.5 ns limit on individual beam pulse lengths available at Omega. Four

or five of the remaining beams drive two Ti point-backlighters, which shine through two 50 μm pinholes [11]. The characteristic 4.7 keV Ti He α radiation projects 2 radiographs of the thin-shell capsule through viewports on the hohlraum onto a two-frame gated camera. One pinhole is illuminated around 3 ns, and the other is illuminated around 7 ns, to produce two snapshots of the thin shell as it implodes. The overall time resolution is 240 ps, and the magnification of the image has varied from 5 to 8. The viewports on the hohlraum are covered with 0.5 μm of Au to keep up the albedo and thus reduce the asymmetry effect of the viewport holes on the capsule.

Over the past two years, we have improved our image quality. Backlit pinholes produce a much higher signal/noise ratio than area backlighters [11], because one can use a smaller backlighter spot size, which in turn allows for a much higher backlighter intensity for a given laser power. By dividing our images by the flat field of the detector, we have gained an additional 20% improvement in the measurement of the position of the limb. Fig. 7 shows two pictures of one capsule taken 4 ns apart.

The limb position is analyzed as a function of angle. The polar averaged observed width of the limb, shown in Fig. 8, is consistent with our simulation with 50 μm pinholes. We extract the minimum position of the limb as a function of angle, as shown in Fig. 9. This figure shows early (3.7 ns) and late-time (6.7 ns) limb position data vs. angle from a 15 μm shell (shot 19083). Fig. 10 displays the 6.7 ns data with Legendre fits with and without mode 6 included. Clearly, including mode 6 improves the fit. Fig. 11 compares late-time (6.7 ns) limb position data vs. angle with a 2-D integrated radiation-hydrodynamic simulation [3]. There is good qualitative correspondence of various features between experiment and simulation, and in particular, both show a 5-10 μm

positive $a_6$ component corresponding to a –2.5 to -5% average $P_6$. The data and simulation show the following coefficients, in mm, in table 2 below.

## V. Error analysis

There are three main sources of error in the measurements. The error in a specific Legendre mode, $\sigma_l$, due to a random measurement error $\sigma_{rms}$ is given by

$$\sigma_l \equiv \frac{\Delta a_l}{a_0} \approx \frac{\sqrt{2l+1}\,\sigma_{\text{rms}}}{\text{d}\sqrt{\text{n}}} \qquad (2)$$

where n is the number of independent measurements and d is the distance traveled by the shell. The $\sqrt{2l+1}$ term arises from the fact that the Legendre mode $P_l$ has an rms of $1/\sqrt{2l+1}$. In our experiments on Omega, $\sigma_{rms}$= 2 μm, n = 100, and d is typically 200 μm. Thus the random error for a given Legendre coefficient $a_l/a_o$ is then $\sqrt{2l+1}$ 0.1%.

Another source of error comes from fabrication defects. If the thin shell has a 1% variation in thickness or density, then the distance moved will also vary by about 1%. Current capsules have a thickness variation of 0.2 to 0.8 μm out of a total thickness of 15 μm, almost entirely in a $P_1$ defect – like an off-centered sphere. A pure $P_1$ defect will not affect the measurements because to first order it is equivalent to a displacement of the center of the image, and we remove this defect before we analyze our data. We currently do not know the spectrum of thickness variations, but we plan to measure these variations with interferometry as part of the thin-shell selection process. Based on measurements of the outside radius, it is very likely that for modes 4 and greater, the thickness variations are < 0.1 μm.

A third source of error comes from laser pointing errors and laser power imbalance. Fig. 12 shows the results of calculations made with the 3-D viewfactor code GERTIE. For two of the Omega shots in February 2000, a 10 μm shell (shot 19082) and a 15 μm shell (shot 19083), the actual beam energies of each of the 42 beams entering the hohlraum were taken and used to modulate the power going to the hohlraum wall proportionately. The viewfactor code then calculated the resulting flux on the capsule. The line of sight from the pinhole to the detector defines a great circle around the capsule, which corresponds to the limb as seen in the images. The flux along this limb was then compared in two cases: (1) the full 3-D version and (2) a 2-D version in which each beam became an azimuthally symmetric ring. Fig. 12 compares the 2-D with the 3-D version of the code at 3 ns, near the most sensitive time for the thin shells. Note that the 2-D and 3-D versions are similar for shot 19083, but not for shot 19082. In shot 19082, one of the beams had only 130 J, compared to the average of all the other beams of 248 J. This particular beam, unfortunately, was on the limb relative to the line of sight, at an angle of 316°. This accounts for the large negative feature at around 300° seen in the 3-D calculation. Thus the thin-shell technique requires decent power balance, which of course will also be a requirement for ignition on NIF.

The two shots differed in one other significant way as well. Shot 19083, with the 15 μm thick shell, showed a random measurement error of 3.0 μm at 6.7 ns, whereas shot 19082, with the 10 μm thick shell, showed a random measurement error of 7.3 μm at 6.7 ns. We believe this suggests that the thinner shell started breaking up due to the Rayleigh-Taylor instability [12], whereas the thicker shell remained intact.

## VI. Extension to NIF

To apply Eq. (2) to the effect of random measurement errors on NIF, we need to calculate how the shell travel distance d scales with different drives. To calculate a rough value for d, we employ a simple model in which the acceleration g is constant. Then $d = 0.5\ gt^2$, with g proportional to ablation pressure / ρh, with h the thickness of the shell. The ablation pressure is proportional to the radiation drive temperature to the 3.5 power [13]**.** Finally, note that the shell thickness h must be thick enough to avoid Rayleigh-Taylor breakup of the shell; thus d/h must be some fixed value c [12]. Substituting d= c h yields the relation $d \sim T^{1.75} t$. Table 3 below makes use of this relationship to give the expected sensitivity of the thin shell technique on NIF. On the foot (peak), d = 240 (715) μm. This means that if we have the same random measurement error of 2 μm on NIF, we have an expected measurement accuracy on the foot (peak) of $\sqrt{2l+1}$ 0.1 (0.03) %. This is a factor of two better than what is required for meeting the NIF specification of 0.25% for $P_8$, the most stringent case.

Since the sensitivity of the thin shell is peaked near shock break-out time, one would sample different episodes of the NIF drive by using a variety of shell thicknesses h spanning the range one can infer from Table 3 (i.e. from ≈15 to ≈ 60 μm).

With perfect power balance and pointing, NIF will have 16 beams evenly spaced in azimuth in three planes: the hohlraum symmetry plane at the center, and one halfway between the symmetry plane and the laser entrance hole on each side. We expect roughly 50% modulation of intensity on the hohlraum wall, which (from viewfactor calculations) translates to less than 0.2% modulation on the capsule. This is good enough that we can

consider the illumination to be 2-D. Then our measurements of the Legendre coefficients will be meaningful. The expected 10% power imbalance per beam and 50 μm pointing errors results in a flux asymmetry on the capsule of 0.9, 0.8, 0.7, 0.4, and 0.15% rms for modes 1-5, and less than 0.07% for all remaining modes. This will limit our measurements of the "intrinsic" $a_2$ and $a_4$ Legendre coefficients to these values of 0.8% and 0.4%. If the power balance and pointing errors are much worse than expected, we will see the effect of these errors in our measurements.

## VII. Conclusions

Our current OMEGA experimental campaign is developing the thin shell diagnostic for use on NIF with the needed accuracy. The thin shell diagnostic has the advantage of linearity over alternative measurement techniques, so low-order modes will not corrupt the measurement of high-order modes. As a demonstration of the utility of the technique, we have successfully designed an experiment to detect the higher order $P_6$ mode. Although our current random measurement errors are adequate, better comparisons of current data with simulations would require 3D codes. A better approach planned for the future is to take advantage of improvements in power balance at Omega to gather better data for which 2D modeling is sufficient. In addition, we will step up efforts for more thorough characterization of thin shell thickness uniformity. Other planned improvements include switching to a single gated frame per shot to provide more signal and more magnification, leading to better signal-to-noise; switching to a Gd patch instead

of a Au patch for a 3x increase in Ti backlighter throughput; and implementing an improved alignment strategy for the backlit pinhole technique. We also hope to use the thin shell technique to quantify shifts and improvements in symmetry from using higher albedo hohlraum wall mixtures [14].

## VIII. Appendix: Spectrum Scaling

Fig. 13 shows the flux from the hohlraum wall of a typical NIF simulation at 5 ns, towards the end of the foot, as a function of angle as seen from the hohlraum center. The lack of flux near 0° comes from the laser entrance hole, and the peak around 40° is x-ray emission resulting from the outer ring of laser beams. Fig. 14 shows the spectrum of this wall flux as Legendre coefficient vs. mode number. This spectrum scales roughly as mode number $^{1/2}$, at least to mode numbers of 100 or so. Fig. 15 shows the radiation transfer function for a capsule/case ratio of 0 and 0.4. This function scales like mode number$^{-5/2}$. Fig. 16 shows the expected flux asymmetry spectrum on the capsule, which is the hohlraum wall spectrum times the radiation transfer function. This spectrum scales roughly as mode number$^{-3}$. Fig. 16 also shows the NIF specifications, which scales more slowly as mode number$^{-1}$. This comparison shows that we need only be concerned with mode numbers less than or equal to 8.

## Acknowledgements

We thank the Laboratory for Laser Energetics, University of Rochester, for the use of the Omega laser. We also thank the referee for his clarifying comments.

This work was performed under the auspices of the U.S. Department of Energy by the Lawrence Livermore National Laboratory under Contract No. W-7405-ENG-48.

## References

[1] J.D. Kilkenny, T.P. Bernat, B.A. Hammel et al, "Lawrence Livermore National Laboratory's Activities to Achieve Ignition by X-Ray Drive on the National Ignition Facility", Laser and Part. Beams **17**(2), 159-171 (1999), and J.D. Kilkenny, E.M. Campbell, J.D. Lindl et al, "The Role of the National Ignition Facility in Energy Production From Inertial Fusion", Phil. Trans. Royal Soc. of London **357**(1752), 533-553 (1999); and J.A. Paisner, J.D. Boyes, S.A. Kumpan, jW.H. Lowdermilk, M.S. Sorem, Laser Focus World 30, 75 (1994).

[2] S.M. Pollaine, "Radiation Transport Between Two Concentric Spheres", Nuclear Fusion 40, 2061 (2000).

[3] G.B. Zimmerman and W.L. Kruer, "Numerical Simulation of Laser-Initiated Fusion", Comments Plasma Phys. Control. Fusion **2**, 51-61 (1975).

[4] S.W. Haan, private communication.

[5] N.D. Delamater, G.R. Magelssen and A.A. Hauer, "Reemission technique for symmetry measurements in Hohlraum targets containing a centered high-Z ball", Phys. Rev. E **53**, 5240 (1996).

[6] P. Amendt, S.G. Glendinning, B.A. Hammel, O. Landen, and L.J. Suter, "Direct Measurement of X-Ray drive from Surrogate Targets in Nova Hohlraums", Phys. Rev. Lett. **77**, 3815 (1996).

[7] S.M. Pollaine, M.M. Marinak and D.H. Munro, "3-D Simulations of Tetrahedral Hohlraums", Bull. Am. Phys. Soc. **42**, 1993 (1997).

[8] A. Hauer, N. Delamater, D. Ress *et al.*, "Review of drive symmetry measurement and control experiments on the Nova laser system", Rev. Sci.

Instrum. **66**, 672-7 (1995); and N. D. Delamater, T. J. Murphy, A. A. Hauer *et al.*, "Symmetry experiments in gas-filled hohlraums at NOVA", Physics of Plasmas **3**, 2022-8 (1996); R. Turner, P. Amendt, O.L. Landen, S.G. Glendinning, P. Bell, C. Decker, B.A. Hammel, D. Kalantar, D. Lee, *et. al.*, "Demonstration of time-dependent symmetry control in hohlraums by drive-beam staggering", Physics of Plasmas **7,** 333-337**,** (2000).

[9] K.O. Mikaelian,"Simple model for ablative stabilization", Phys. Rev. A 46, 6621 (1992); D. Colombant, W. Manheimer, and E. Ott, "Three-Dimensional, Nonlinear Evolution of the Rayleigh-Taylor Instability of a Thin Layer", Phys. Rev. Lett. **53**, 446. (1984).

[10] P. Amendt, A. Shestakov, O. Landen, S. Pollaine, D.K. Bradley, L. Suter and R.E. Turner, "Implosion target surrogacy studies on Omega for the National Ignition Facility: backlit thinshells", submitted to Phys. PLasmas (2001).

[11] O. L. Landen, D.R. Farley, S.G. Glendinning, L.M. Logory, P.M. Bell, J.A. Koch, F.D. Lee, D.K. Bradley, D.H. Kalantar, C.A. Back, and R.E. Turner, "X-Ray Backlighting for the National Ignition Facility", Rev. Sci. Instrum. **72**, 627-634 ( 2001); A. B. Bullock, O.L.Landen, and D.K. Bradley, "10 μm and 5 μm Pinhole-Assisted Point-Projection Backlit Imaging for the National Ignition Facility", Rev. Sci. Instrum. **72**, 690-693 (2001).

[12] D.L. Youngs, "Numerical Simulation of turbulent Mixing by Rayleigh-Taylor Instability", Physica 12D, 32-44 (1984); K.I. Read, "Experimental Investigation of Turbulent Mixing by Rayleigh-Taylor Instability", Physica 12D, 45-48 (1984).

[13] J. Lindl, “Development of the indirect-drive approach to intertial confinement fusion and the target physics basis for ignition and gain”, Physics of Plasmas **2**(11), 3933-4024 (1995).

[14] H. Nishimura, T Endo, H. Shiraga, Y. Kato and S. Nakai, “X-ray emission from high-Z mixture plasmas generated with intense blue laser light”, Appl. Phys. Lett. **62**(12), 1344-1346 (1993); and T.J. Orzechowski, M.D. Rosen, H.N. Kornblum et al, “The Rosseland Mean Opacity of a Mixture of Gold and Gadolinium at High Temperatures”, Phys. Rev. Lett. **77,** 3545 (1996).

**Table 1.** Experimental accuracy demonstrated at Nova/Omega, scaled to NIF, for the four asymmetry diagnostics discussed in this paper. The first column is the accuracy to a $P_2$ perturbation that lasts for 2 ns, either on the foot or at the peak. The remaining columns show both the accuracy to a perturbation that lasts for the entire length of the XSfoot (top value), and the response to the perturbation being constant for all time (bottom value in parenthesis).

| | $P_2$,2 ns Foot (peak) | $P_2$ Foot only (all time) | $P_4$ Foot only (all time) | $P_6$ Foot only (all time) | $P_8$ Foot only (all time) |
|---|---|---|---|---|---|
| ~~NIF ignition requirement~~ | ~~10%~~ (10%) | ~~2%~~ (1%) | ~~1%~~ (0.5%) | ~~0.7%~~ (0.33%) | ~~0.5%~~ (0.25%) |
| Reemission ball | 3% | | | | |
| Foam Ball | 5% (2.5%) | 0.5% (0.5%) | 0.6% (0.6%) | | |
| Imploded Core | NA | 0.25% (0.25%) | | | |
| Thin Shell | NA | 0.5% | 0.6% | 0.7% | 0.8% |

**Table 2.** Comparison of Legendre coefficients in microns between data and simulation.

| | data | simulation |
|---|---|---|
| $a_2$ | -7.6 | -2.7 |

| | | |
|---|---|---|
| $a_4$ | -6.2 | -7.7 |
| $a_6$ | 10.0 | 5.0 |
| $a_8$ | -2.7 | 0.0 |

**Table 3.** An extension of the Omega parameters to NIF for similar-density shells shows that if we eliminate systematic errors, and can maintain 2 μm accuracy in each measurement of limb position, then we can accurately measure asymmetry to better than NIF specifications.

| Omega | NIF foot / spec | NIF peak / spec |
|---|---|---|

| | | | |
|---|---|---|---|
| T (eV) | 90 | 86 | 300 |
| t (ns) | 7 | 9 | 3 |
| $(T/100)^{1.75}$ t | 5.8 | 6.9 | 20.5 |
| d(μm) | 200 | 240 | 715 |
| $P_2$ sensitivity | 0.22% | 0.19% / 3 % | 0.06% / 1% |
| $P_8$ sensitivity | 0.41% | 0.34% / 0.75% | 0.12% / 0.25% |

## Figure Captions

Fig. 1. NIF ignition capsule and its radiation drive temperature

Fig. 2. Yield of NIF ignition capsule as a function of applied flux asymmetry in P6 (solid) and P8 (dashed) for foot only and for all time. NIF specifications have adequate margin for error.

Fig. 3. NIF flux asymmetry as a function of time from an integrated radiation hydrodynamic simulation. This simulation has not been fully optimized for flux symmetry.

Fig. 4. Sensitivity at 8 ns to a pulse of flux asymmetry at earlier time t, as a function of t. Note that the sensitivity jumps sharply right at shock break out time.

Fig. 5. Radiation transfer function as a function of mode number for various capsule/case radii ratios. Note the huge enhancement in modes 6 and 8 in going to capsule/case = 0.6.

Fig. 6. Schematic of our experiment, and a picture of the hohlraum with its thin-shell capsule, with capsule/case = 0.6. Later experiments have capsule/case = 0.5, and 0.5 mm of gold over the viewport to improve albedo.

Fig. 7 Picture of the same thin shell 4 ns apart.

Fig. 8. An azimuthally averaged capsule limb profile, showing transmission of 4.7 keV radiation vs. radius of capsule.

Fig. 9. Early and late time limb position vs. angle. The late time image is folded over four times to display only even Legendre modes on the right.

Fig. 10. The data from 0° to 360° is folded over 4 times, and compared with fits to $P_0$, $P_2$ and $P_4$ (dashed), and $P_0$, $P_2$, $P_4$ and $P_6$ (solid).

Fig. 11. A comparison of limb position data (dots) vs. polar angle with a 2-D integrated radiation-hydrodynamic simulation (red line) from shot 19083.

Fig. 12. Viewfactor simulations using the actual power in each of the 42 beams that went into the hohlraum for shots 19082 (left) and 19083 (right). The 2D dashed curves were made by azimuthally averaging each laser beam.

Fig. 13. Flux from hohlraum wall vs. angle from the hohlraum center. The laser entrance hole is at 0° and the outer NIF beams hit at 40°.

Fig. 14. Spectrum of flux pattern shown in Fig. 13 vs. mode number, normalized to total flux. This spectrum scales roughly as mode number$^{-1/2}$.

Fig. 15. Radiation transfer function from wall to capsule for sphere within a sphere for capsule/case ratios of 0 (straight line) and 0.4. Transfer function for sphere in cylinder mixes modes, but the decrease follows same power law, namely mode number$^{-2.5}$.

Fig. 16. Flux asymmetry spectrum on capsule is roughly the product of the wall spectrum (Fig. 14) times the radiation transfer function (Fig. 15), and goes like mode number $^{-3}$. The NIF specifications (straight line) go like mode number$^{-1}$.

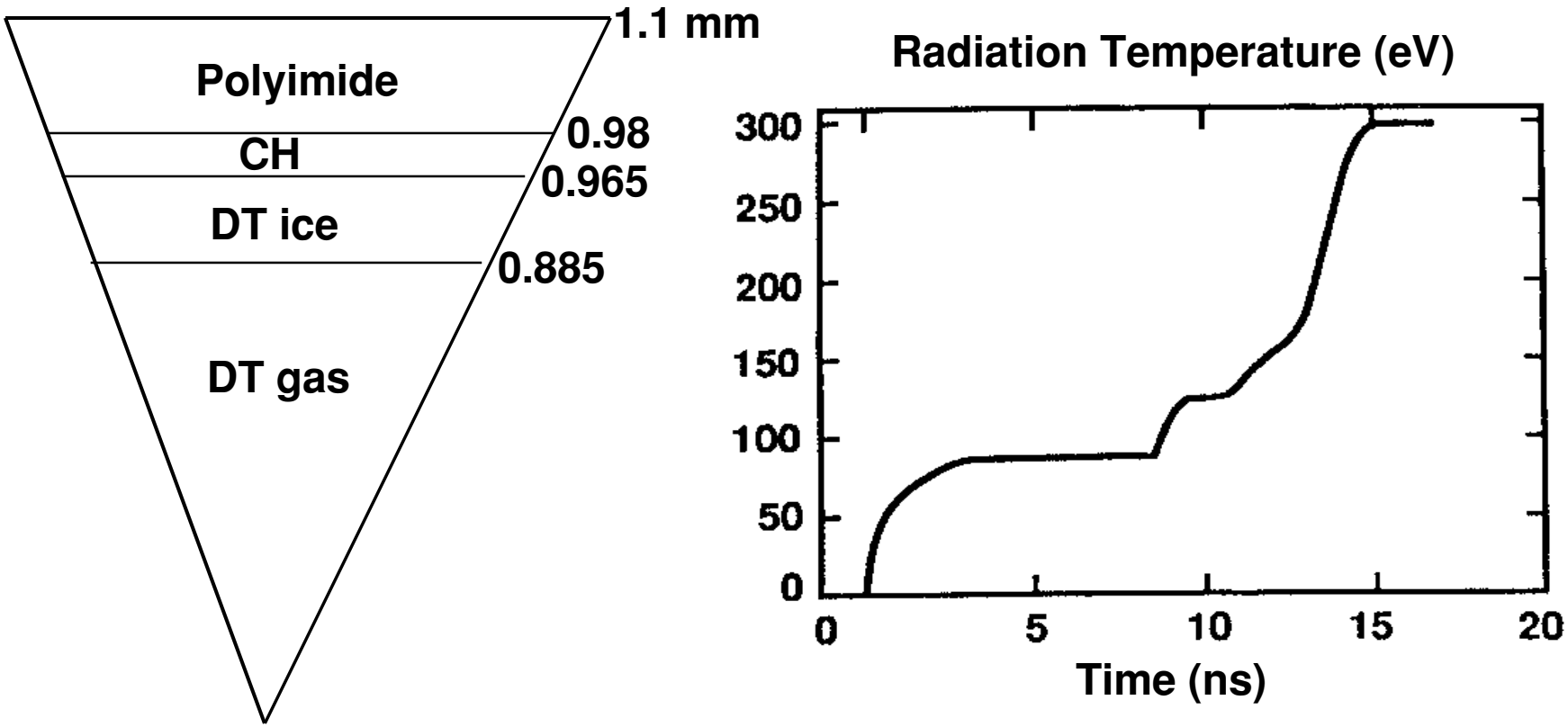


**Fig. 1. NIF ignition capsule and its radiation drive temperature**

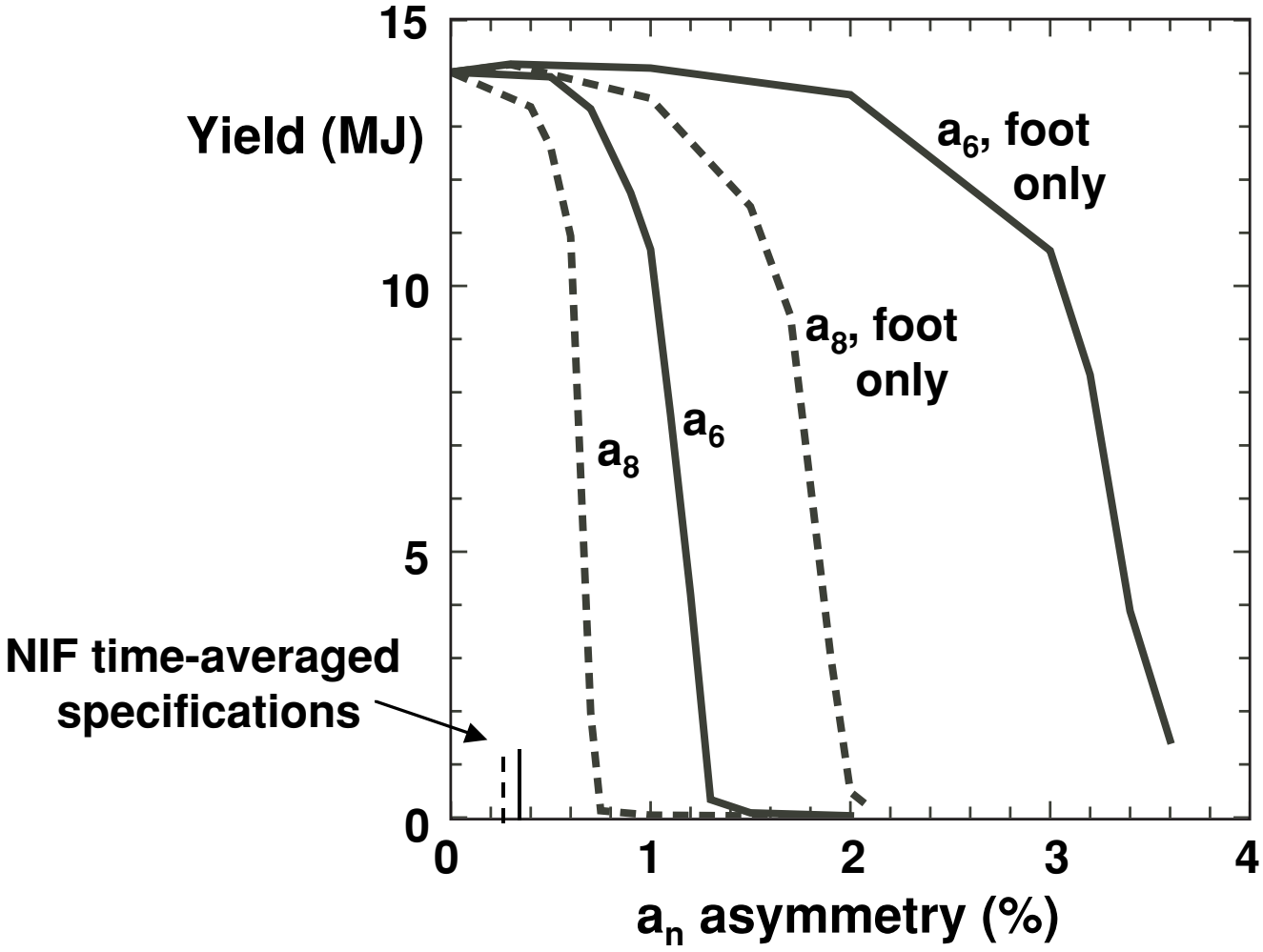


**Fig. 2. Yield of NIF ignition capsule as a function of applied flux asymmetry in $P_6$ (solid) and $P_8$ (dashed) for foot only and for all time. NIF specifications have adequate margin for error.**

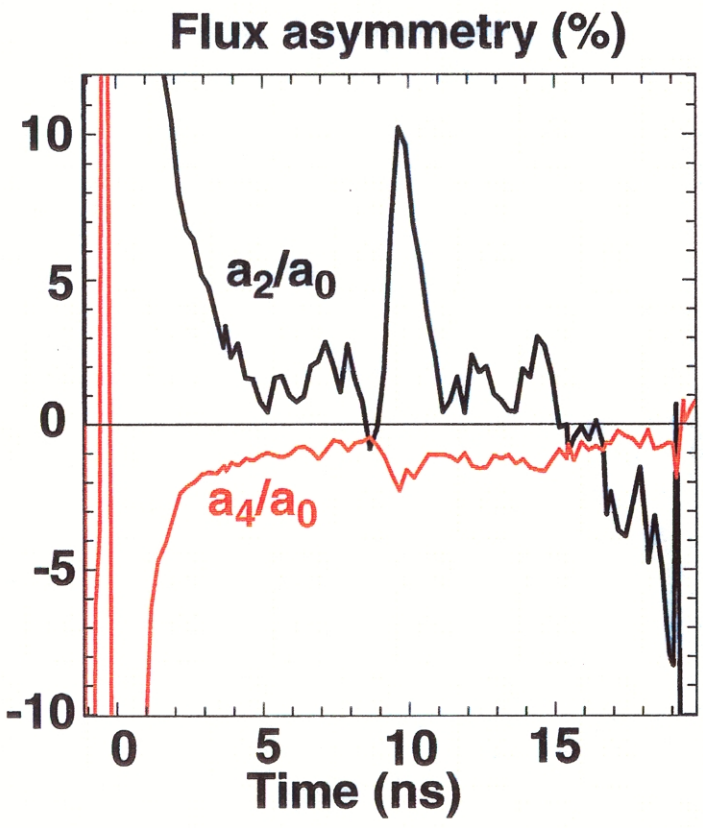


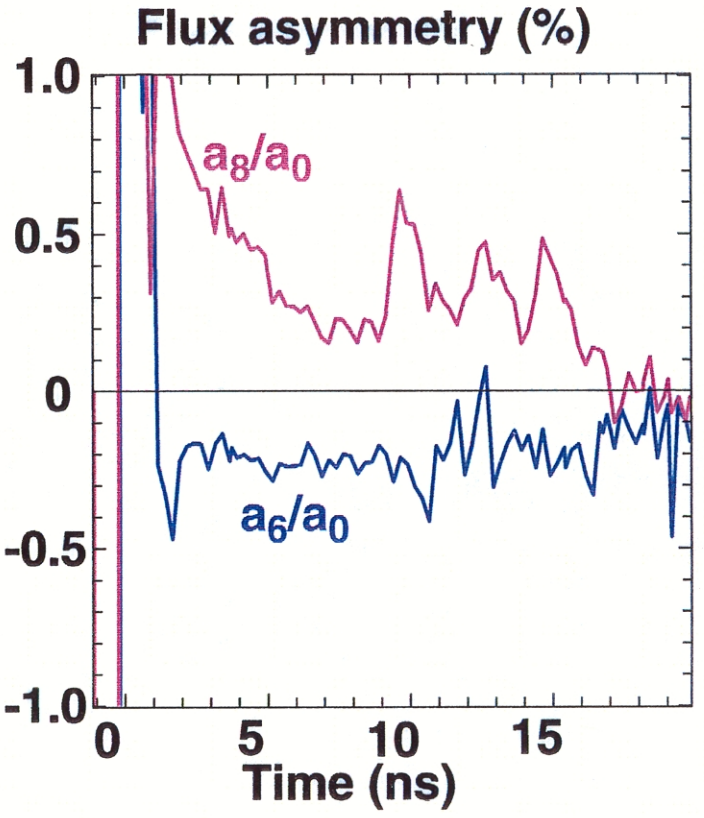


**Fig. 3. NIF flux asymmetry as a function of time from an integrated radiation hydrodynamic simulation. The simulation has not been fully optimized for flux symmetry.**

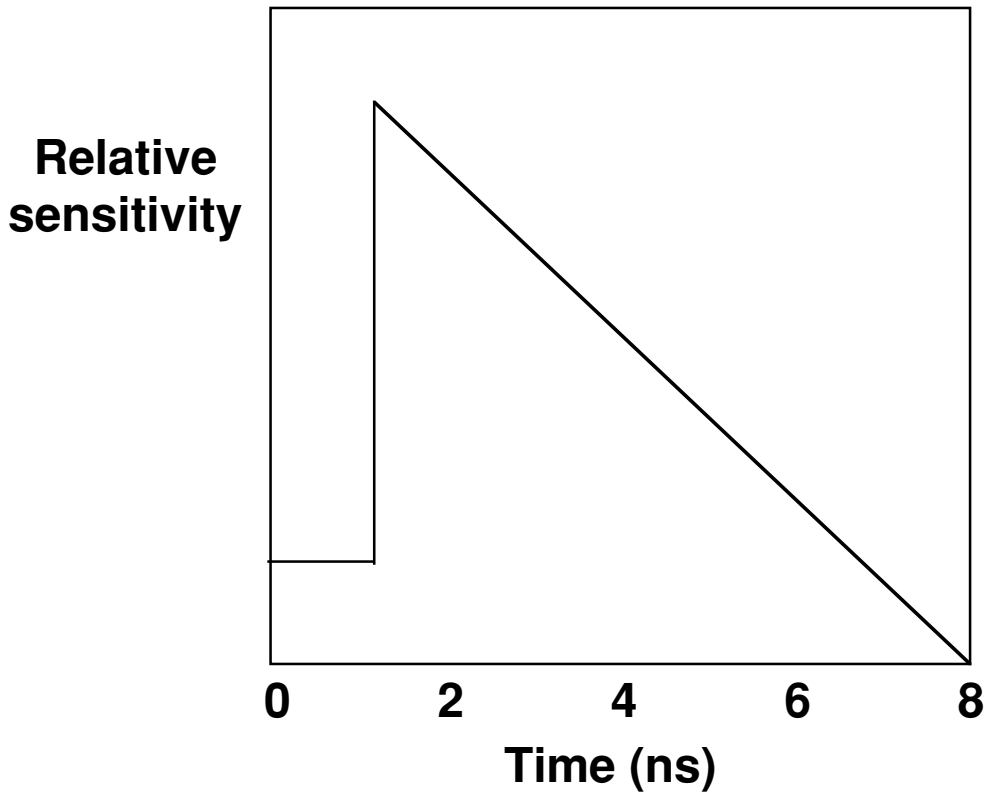


**Fig. 4. Sensitivity at 8 ns to a pulse of flux asymmetry at earlier time t, as a function of t. The sensitivity jumps sharply right at shock breakout time (1.4 ns).**

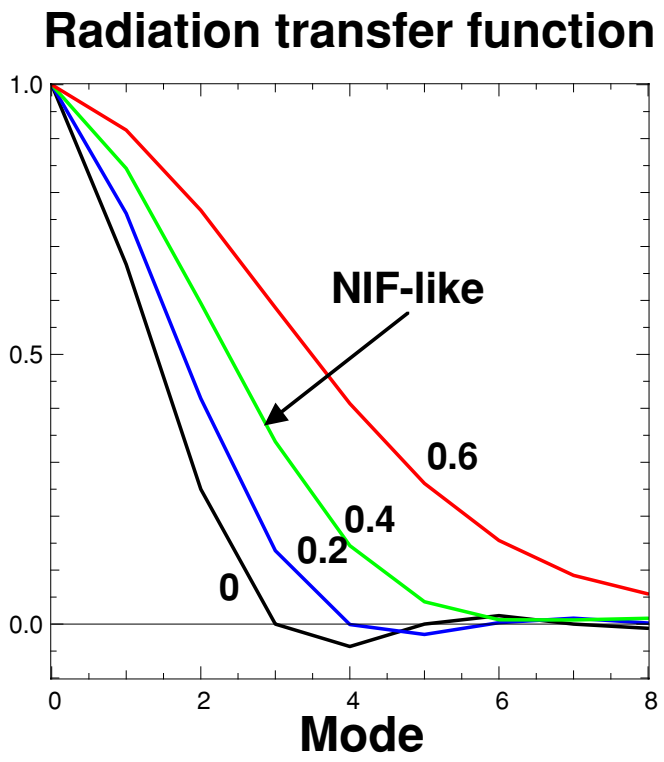


**Fig. 5. Radiation transfer function as a function of mode number for various capsule/case radii ratios. Note the huge enhancement in modes 6 and 8 with capsule/case = 0.6.**

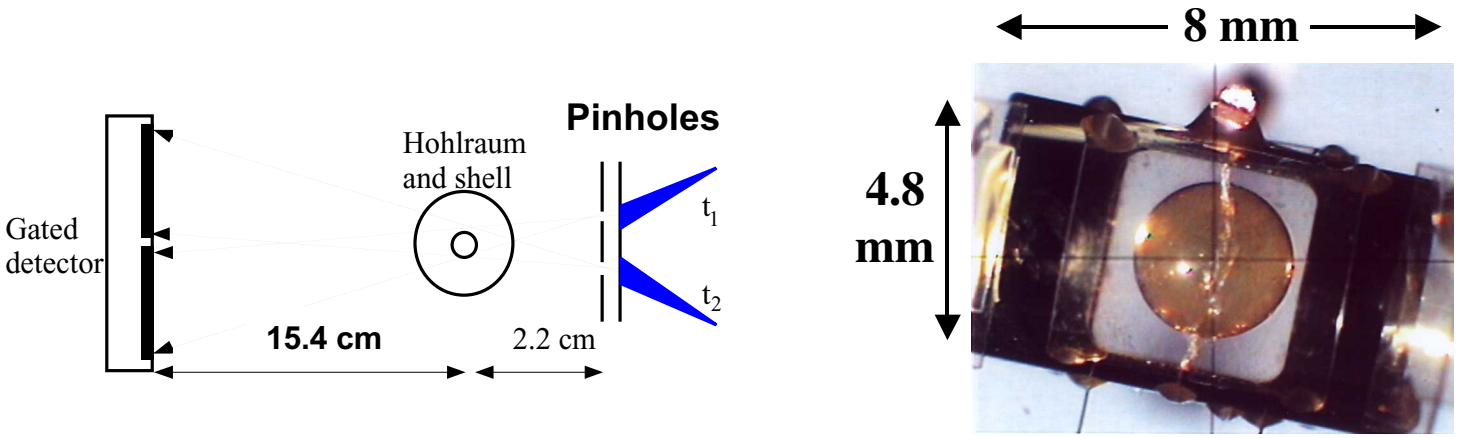


**Fig. 6. Schematic of our experiment, and a picture of the hohlraum with its thin-shell capsule, with capsule/case = 0.6. Later experiments have capsule/case = 0.5, and 0.5 μm of gold over the viewport to improve albedo.**

**Fig. 7. Pictures of the same thin shell 4 ns apart.**

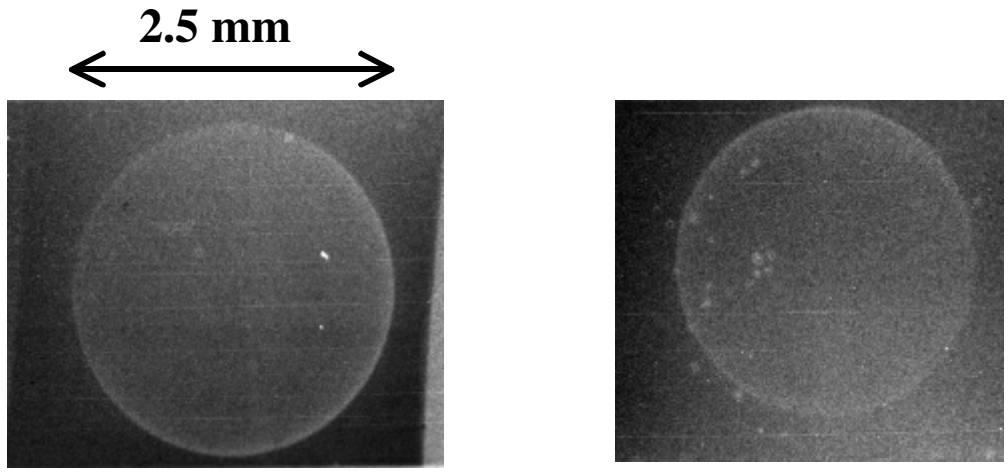

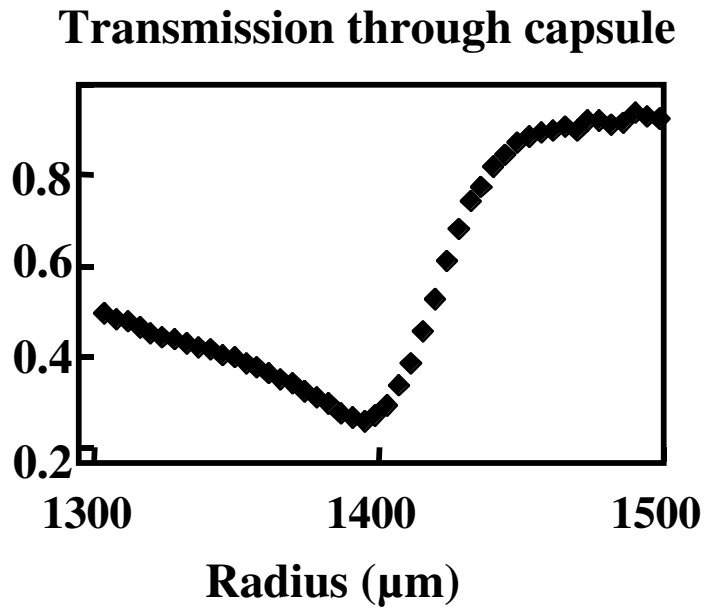


**Fig. 8. An azimuthally averaged capsule limb profile, showing transmission of 4.7 keV radiation vs. radius of capsule.**

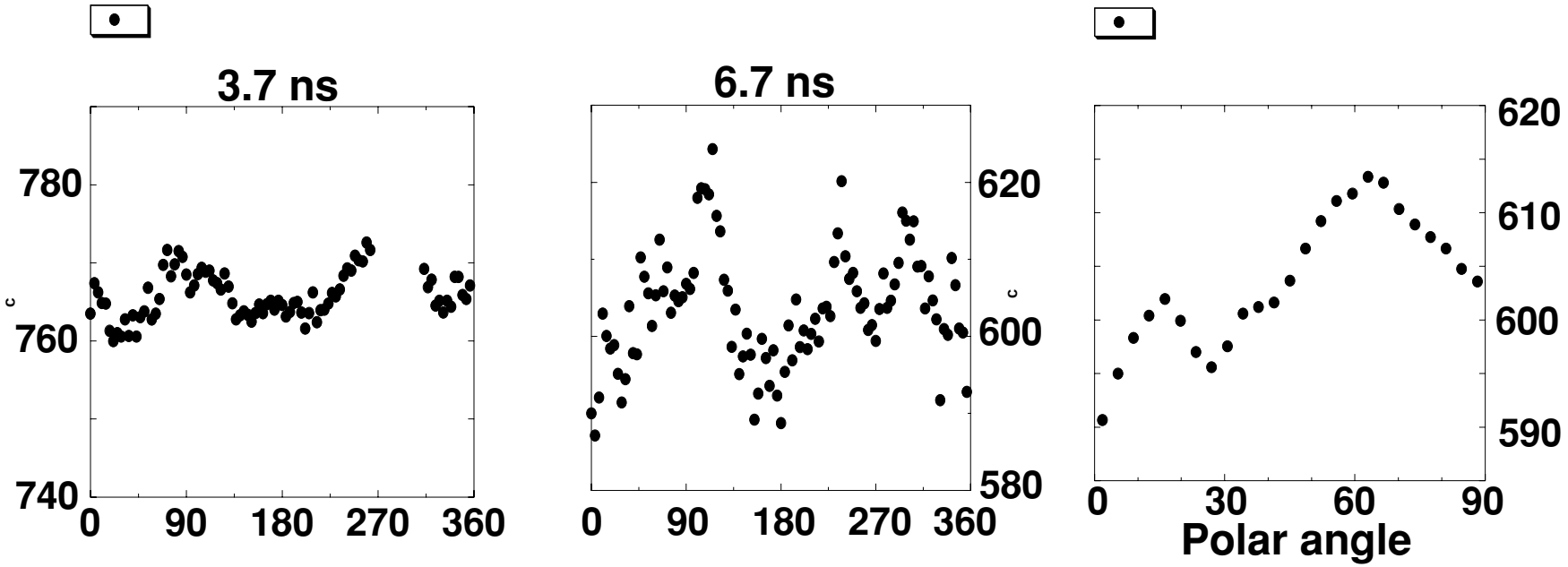


**Fig. 9. Early and late time limb positions vs. angle. The late time image is folded over four times to display only even Legendre modes on the right.**

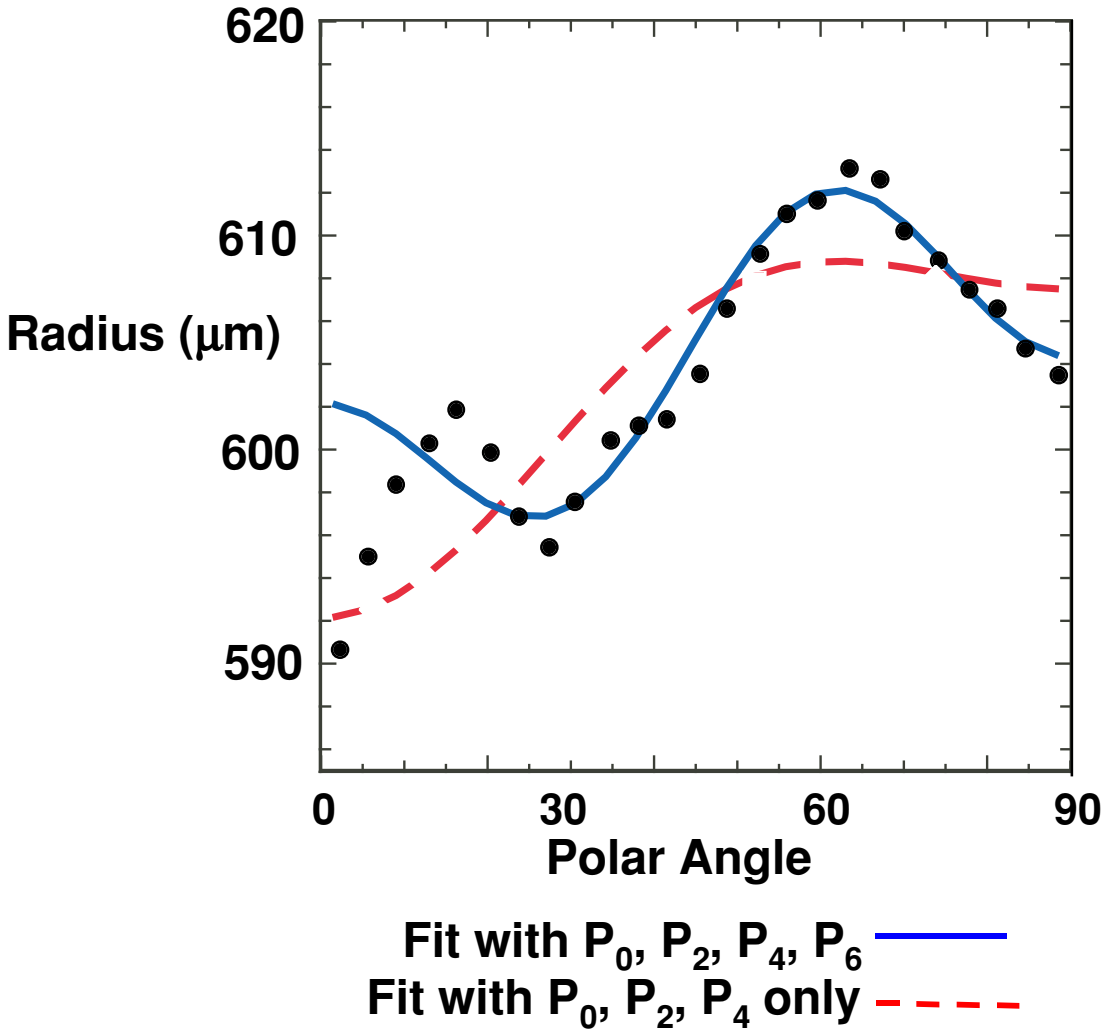


FIG. 10. The data from 0º to 360º is folded over 4 times, and compared with fits to $P_0$, $P_2$ and $P_4$(dashed), and $P_0$, $P_2$, $P_4$ and $P_6$(solid).

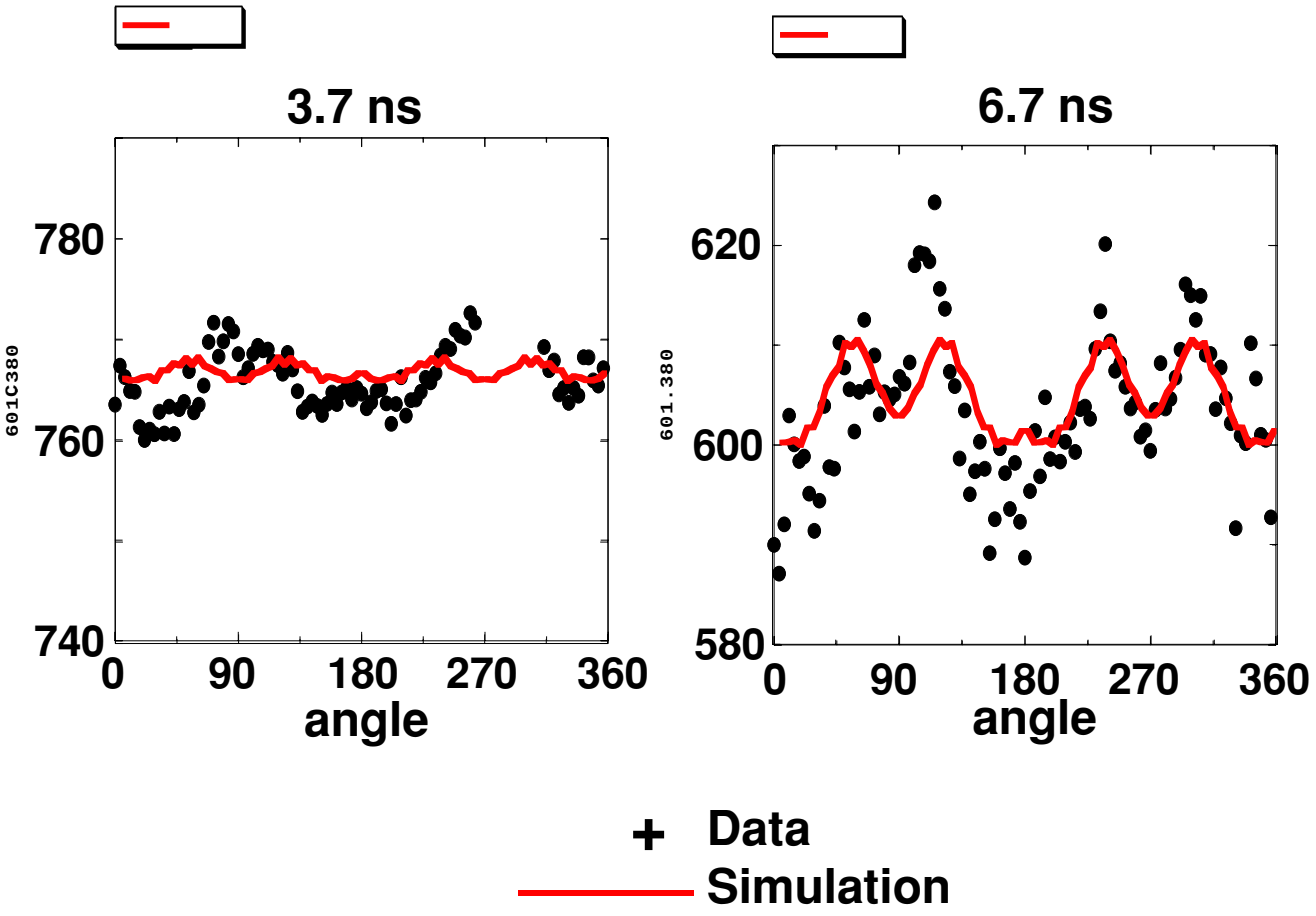


**Fig. 11. A comparison of limb position data (dots) vs. polar angle with a 2-D integrated radiation hydrodynamic simulation (line) from shot 19083.**

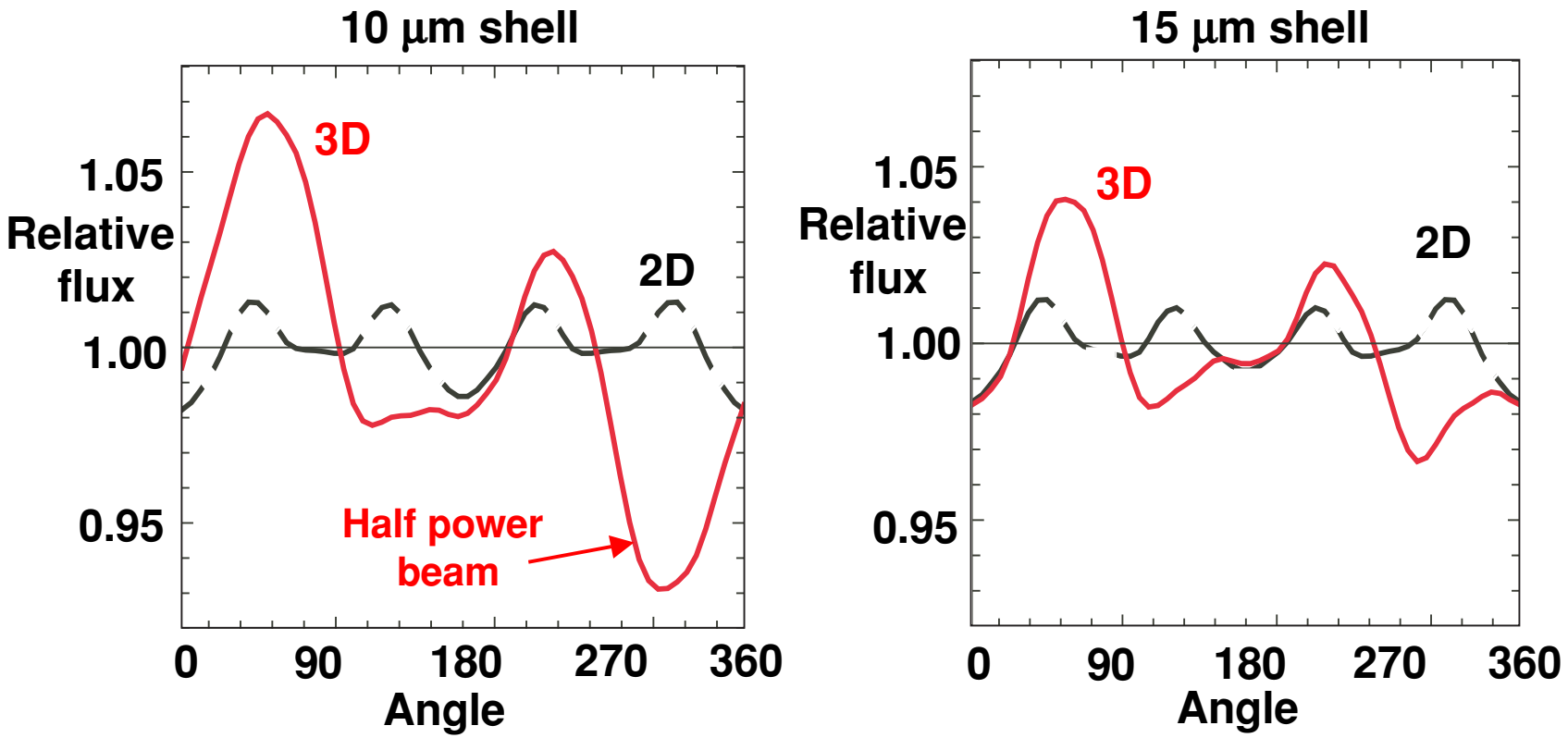


Fig. 12. Viewfactor simulations using the actual power in each of the 42 beams that went into the hohlraum for shots 19082 (left) and 19083 (right). The 2D dashed curves were made by azimuthally averaging each laser beam.

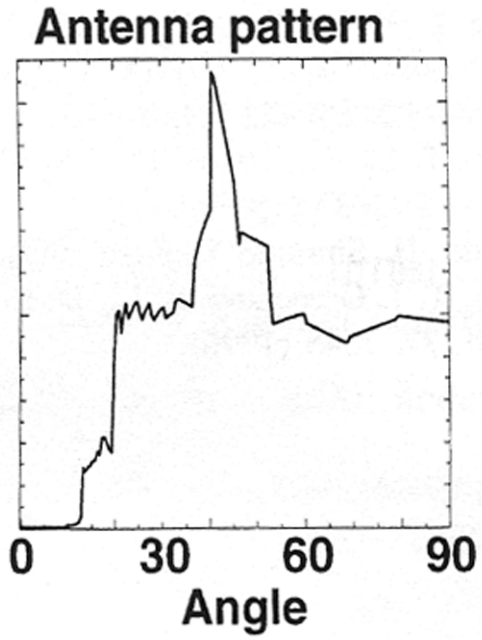


Fig. 13. Flux from hohlraum wall vs angle from the hohlraum center. The laser entrance hole is at 0º and the outer NIf beams hit at 40º.

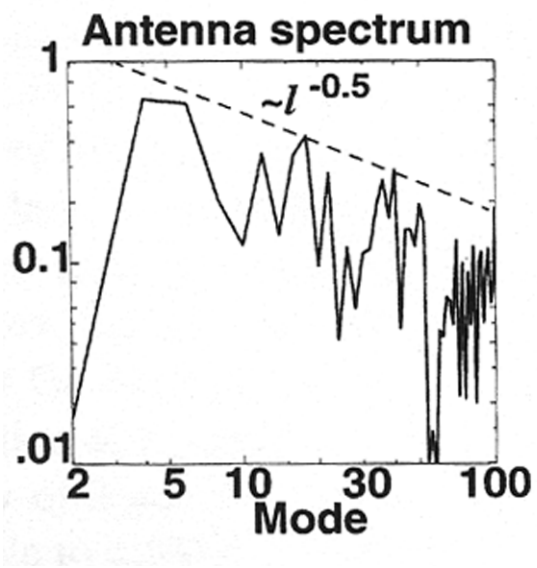


Fig. 14. Spectrum of flux pattern shown in Fig. 13 vs mode number, normalized to total flux. This spectrum scales roughly as mode number $^{-1/2}$.

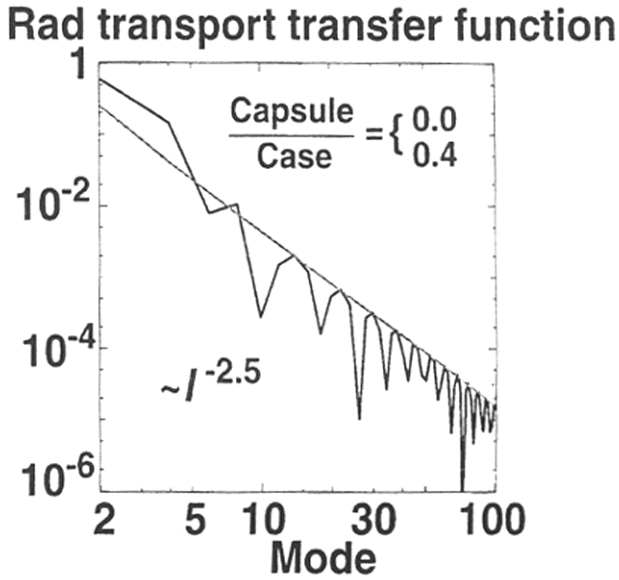


Fig. 15. Radiation transfer function from wall capsule.for sphere within a sphere for capsule/case ratios of 0 (straight line) and 0.4. Transfer function for sphere in cylinder mixes modes, but not decrease follows the same power law, namely mode number $^{-2.5}$.

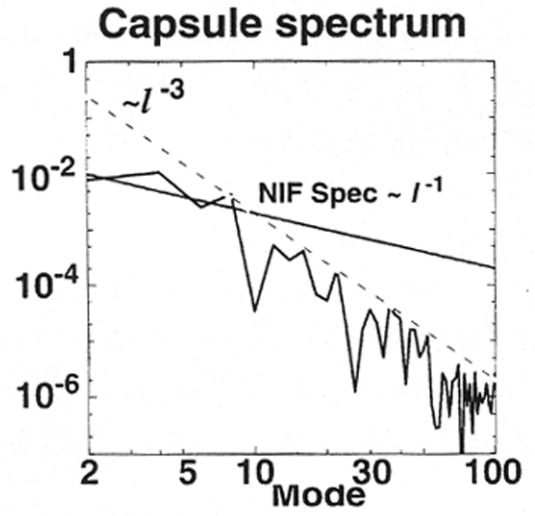


Fig. 16. Flux asymmetry spectrum on capsule is roughly the product of the wall spectrum (Fig. 14) times the radiation transfer function (Fig. 15), and goes like mode number $^{-3}$. The NIF specifications (straight solid line) go like mode number $^{-1}$.